A multiscale model for charge inversion in electric double layers

S. Y. Mashayak and N. R. Aluru[a)]
Department of Mechanical Science and Engineering, Beckman Institute for Advanced Science and Technology, University of Illinois at Urbana-Champaign, Urbana, Illinois 61801, USA

(Received 26 February 2018; accepted 14 May 2018; published online 5 June 2018)

Charge inversion is a widely observed phenomenon. It is a result of the rich statistical mechanics of the molecular interactions between ions, solvent, and charged surfaces near electric double layers (EDLs). Electrostatic correlations between ions and hydration interactions between ions and water molecules play a dominant role in determining the distribution of ions in EDLs. Due to highly polar nature of water, near a surface, an inhomogeneous and anisotropic arrangement of water molecules gives rise to pronounced variations in the electrostatic and hydration energies of ions. Classical continuum theories fail to accurately describe electrostatic correlations and molecular effects of water in EDLs. In this work, we present an empirical potential based quasi-continuum theory (EQT) to accurately predict the molecular-level properties of aqueous electrolytes. In EQT, we employ rigorous statistical mechanics tools to incorporate interatomic interactions, long-range electrostatics, correlations, and orientation polarization effects at a continuum-level. Explicit consideration of atomic interactions of water molecules is both theoretically and numerically challenging. We develop a systematic coarse-graining approach to coarse-grain interactions of water molecules and electrolyte ions from a high-resolution atomistic scale to the continuum scale. To demonstrate the ability of EQT to incorporate the water orientation polarization, ion hydration, and electrostatic correlations effects, we simulate confined KCl aqueous electrolyte and show that EQT can accurately predict the distribution of ions in a thin EDL and also predict the complex phenomenon of charge inversion. *Published by AIP Publishing.* https://doi.org/10.1063/1.5026975

I. INTRODUCTION

The charge inversion is a phenomenon in which the coion charge density exceeds the counterion charge density in a certain region of the electric double layer (EDL). The presence of counterions next to a charged surface reduces the apparent surface charge of the EDL compared with the bare surface charge. The apparent surface charge is the charge that ions away from the surface see. The charge inversion occurs when the apparent surface charge has an opposite sign than that of the bare surface charge. The reversal of the apparent surface charge is possible when the number of counterions next to the surface exceeds the surface charge. In an EDL region that experiences the reversal of the apparent charge, coions are attracted and counterions are repelled, which causes the charge inversion.

Charge inversion gives rise to several counterintuitive phenomena, such as attraction between like-charged surfaces,[1,2] reversal of mobility of charge colloids,[3,4] and electro-osmotic flow reversal phenomena.[5] Furthermore, charge inversion phenomena play a prominent role in biological processes and micro/nano-fluidic applications, such as DNA uptake by the cell for gene therapy,[6] tunable ionic filters,[7] desalination,[8,9] energy storage devices,[10,11] and many other industrial applications. Therefore, understanding the molecular origins of the properties of EDLs and charge inversion phenomena is critical to devise mechanisms to control interfacial phenomena and design novel fluidic functionalities. Variations in the surface-fluid molecular interactions, packing and orientational ordering, thermodynamic, and dynamical properties of fluid molecules across multiple length scales ranging from a few Angstroms to several nanometers govern the behavior of fluidic systems involving interfaces. For example, due to the long-range nature of electrostatics, the local arrangement of ions in the thin EDL near the interface region has strong effects on the electrokinetics at nanometric, micrometric, and even larger scales.[12] Therefore, it is important to study interfacial ionic systems at multiple length-scales.

Experimental investigation of the narrow interfacial region, despite significant progress in new instruments and tools over the past few decades, is still challenging.[13–15] Direct measurements of chemical details in the interfacial region is difficult because fluctuations hinder the ability to separate signal from the interface region over those of the adjacent bulk-like phases. Therefore, theory and computational tools are essential to obtain molecular-level insights of interfaces.

Molecular simulation techniques, such as molecular dynamics (MD) and Monte Carlo (MC) simulations, can be used to study the microscopic properties of interfacial fluids.[16,17] However, it is computationally expensive to perform atomistic simulations due to long equilibration times and extensive phase-space sampling required to compute average properties reliably, i.e., with low statistical noise. For example, MD simulations of electrolyte systems require thousands

[a)]Electronic mail: aluru@illinois.edu

of water molecules per ion and long simulations to achieve reliable statistics. Therefore, the time scales and length-scales accessible by molecular simulations are limited. On the other hand, the classical continuum methods, such as Navier-Stokes equations, are computationally efficient, but fail to accurately describe the atomic-level structure and properties of confined fluids.[18,19] As a result, molecular simulations and classical continuum methods are not applicable for applications that involve multiple time and length scales ranging from the atomic to continuum scales.[20] To address these issues, we need a multiscale method which is not only as accurate as molecular simulations but also as fast as classical continuum methods.

The Gouy-Chapman (GC) theory based on the Poisson-Boltzmann (PB) equation is the most basic and popular theory to study EDL.[21] However, the accuracy of the Gouy-Chapman theory is limited and it cannot predict the charge inversion phenomena. There exist liquid state theories, such as the modified PB theory,[22] integral equation theory,[23] and classical density functional theory (cDFT).[24–29] These theories, in addition to the electrostatic interactions, mainly account for the finite size effects of ions and van der Waals interactions among them. However, they usually ignore molecular details of water and variations in the dielectric permittivity. Interfacial water around ions plays a dominant role in determining the distribution of ions and electrochemical properties of EDLs near charged surfaces.[30] Distinct polar charge distribution of the water molecule gives rise to highly directional intermolecular interactions, strong hydrogen bonding, polarization, and orientational ordering. Near an interface, additional conflicts between surface-water interactions, spatial constraints, and water's tendency to form hydrogen-bonded networks result in microscopic variations in the density, orientation, polarization, dielectric permittivity, and hydration of ions which are widely different from its bulk properties.[31] Therefore, an explicit description of the molecular structure and dielectric and hydration effects of interfacial water is important to study EDLs.

There are some approaches which try to incorporate molecular details of water explicitly. The simplest approach is to model water molecules as hard spheres with uniform dielectric permittivity. The hard sphere water model has been used in various cDFT-based studies of EDL, which is also known as the three-component model (3CM) or molecular solvent model (MSM).[32,33] Lee *et al.*[26] have further incorporated the Lennard-Jones (LJ) interactions among ions, water, and wall particles in the 3CM cDFT. However, the hard sphere model is a very crude approximation for a water molecule and it ignores water-water electrostatic interactions, short-range electrostatic correlations, and variations in the orientation and dielectric permittivity of water. To include water orientation and polarization effects, dipolar solvent-based approaches have been proposed, such as the Langevin dipole model,[34,35] "civilized" solvent model-based cDFT,[36] generic density functional,[37] polar solvation cDFT,[38] and dimer solvent-based cDFT.[39] However, these approaches fail to predict the structural properties of EDLs, such as solvent and ion density profiles and charge inversion phenomena, accurately as compared to fully atomistic molecular simulations.

In Ref. 40, we presented a realistic explicit water based theoretical framework for studying EDLs. The framework is based on an empirical potential-based quasi-continuum theory (EQT)[41–48] and Langevin-Poisson (LP) approach for the electrostatic interactions. In LP-EQT, water polarization and dielectric permittivity variations are modeled using the Langevin dipole approach. Finite size effects of water and ions are modeled using hard sphere approximations. To accurately capture hydration of ions, we systematically developed water-water and ion-water coarse-grained (CG) potentials. We showed that LP-EQT predictions of the water and ion density profiles agree well with those of the reference MD simulations. However, in the LP-EQT approach, we used a mean-field approximation in determining electrostatic interactions. The Langevin-Poisson approach for electrostatics ignores ion-ion, ion-dipole, and dipole-dipole electrostatic correlations.[34]

Electrostatic correlation effects are significant when the ion concentration or the surface charge density or both are high. In particular, the electrostatic correlations give rise to excess interactions between ions which drive the charge inversion.[49,50] Therefore, the focus of this work is to incorporate electrostatic correlation effects in the LP-EQT framework such that LP-EQT can accurately predict the charge inversion phenomena.

The remainder of the paper is organized as follows. In Sec. II, we describe the LP-EQT framework and the model to include electrostatic correlations. In Sec. III, we describe the reference KCl aqueous electrolyte-based charge inversion system. In Sec. IV, we provide the details of systematic coarse-graining to develop a coarse-grained water model and ion-water coarse-grained potentials. In Sec. V A, we discuss the results and limitations of the mean-field electrostatic approach. In Secs. V B and V C, we compute the electrostatic correlations and compare the predictions of densities and charge inversion phenomena from EQT with the reference MD simulations. Finally, we draw conclusions in Sec. VI.

II. THEORY

Consider a mixture of cations (+), anions (−), and water (w) molecules confined in a charged slit channel. At equilibrium, the distribution of the fluid molecules is given by the 1-D Nernst-Planck (NP) equation,

$$\frac{d}{dz}\left(\frac{d\rho_i}{dz} + \frac{\rho_i}{k_B T}\frac{dU_i}{dz}\right) = 0 \tag{1}$$

with boundary conditions

$$\rho_i(0) = 0, \tag{2a}$$

$$\rho_i(L) = 0, \tag{2b}$$

$$\frac{1}{L}\int_0^L \rho_i(z)\,dz = \rho_{i,\text{avg}}, \tag{2c}$$

where ρ_i and U_i are the density and total potential of the molecule i (= +, −, w), respectively, T is the fluid temperature, k_B is the Boltzmann constant, L is the channel width, $\rho_{i,\text{avg}}$ is the average density of the molecule i inside the channel, and

the z-axis is normal to the wall. The solution of Eqs. (1) and (2) is equivalent to the solution of the Boltzmann distribution equation,

$$\rho_i(z) = \rho_{i,\text{ref}} \exp\left(-\frac{U_i(z) - U_{i,\text{ref}}}{k_B T}\right), \tag{3}$$

where $\rho_{i,\text{ref}}$ and $U_{i,\text{ref}}$ are the reference density and potential of the molecule i, respectively. For the electrolyte system, the total potential energy can be split into the electrostatics, $U_{i,\text{elec}}$, and van der Waals (vdW), $U_{i,\text{vdw}}$, contributions as

$$U_i(z) = U_{i,\text{elec}}(z) + U_{i,\text{vdw}}(z). \tag{4}$$

A. vdW potential

The vdW potential has two parts: the wall-fluid, $U^{\text{wf}}_{i,\text{vdw}}$, and fluid-fluid, $U^{\text{ff}}_{i,\text{vdw}}$,

$$U_{i,\text{vdw}}(z) = U^{\text{wf}}_{i,\text{vdw}}(z) + U^{\text{ff}}_{i,\text{vdw}}(z). \tag{5}$$

In the continuum approximation, we represent the wall as a continuous medium with a uniform particle density, ρ_{wall}. Then, the wall-fluid vdW potential is determined as

$$U^{\text{wf}}_{i,\text{vdw}}(\boldsymbol{r}) = \rho_{\text{wall}} \int u^{\text{wf}}_i(r) d\boldsymbol{r}', \tag{6}$$

where $u^{\text{wf}}_i(r)$ is the effective vdW pair potential between the wall atoms and molecule i, $\boldsymbol{r}$ and $\boldsymbol{r}'$ are the position vectors, and $r = |\boldsymbol{r} - \boldsymbol{r}'|$. A procedure to compute $U^{\text{wf}}_{i,\text{vdw}}(\boldsymbol{r})$ for a slit-channel system is described in Ref. 44. Note that in Eq. (6), $\boldsymbol{r} = x\boldsymbol{i} + y\boldsymbol{j} + z\boldsymbol{k}$ is a general position vector. In the case of a 1-D slit channel, the system is periodic in x and y dimensions and therefore, we consider only the z-variations of the properties, i.e., $U^{\text{wf}}_{i,\text{vdw}}(\boldsymbol{r}) = U^{\text{wf}}_{i,\text{vdw}}(x, y, z) = U^{\text{wf}}_{i,\text{vdw}}(z) \,\forall\, x, y$.

The fluid-fluid vdW potentials are more challenging to compute than the wall-fluid potentials. They give rise to the finite size, i.e., excluded volume effects, dispersion attraction, and particle-particle correlations in the fluid. The exact theoretical framework, which accounts for all the fluid-fluid interaction effects, is unknown. In this work, we split the fluid-fluid vdW potential into purely repulsive and dispersion components as

$$U^{\text{ff}}_{i,\text{vdw}}(\boldsymbol{r}) = U^{\text{ff}}_{i,\text{hs}}(\boldsymbol{r}) + \sum_{j=1}^{3} \int_{R^{\text{ff}}_{ij,\text{min}}}^{R^{\text{ff}}_{ij,\text{cut}}} \rho_j(\boldsymbol{r}') u^{\text{ff}}_{ij}(r) d\boldsymbol{r}', \tag{7}$$

where $u^{\text{ff}}_{ij}(r)$ is the effective vdW pair potential between fluid molecules i and j and $R^{\text{ff}}_{ij,\text{min}}$ and $R^{\text{ff}}_{ij,\text{cut}}$ are the inner and outer cutoffs for the dispersion part of the pair potential, respectively. In Eq. (7), $U^{\text{ff}}_{i,\text{hs}}(\boldsymbol{r})$ is the purely repulsive component of the fluid-fluid interactions, which mainly accounts for the excluded volume effects. We use the hard sphere fluid approximation based on the White-Bear version of fundamental measure theory (FMT) mark II[51] to determine $U^{\text{ff}}_{i,\text{hs}}(r)$ as

$$U^{\text{ff}}_{i,\text{hs}}(\boldsymbol{r}) = k_B T \sum_{\alpha} \int d\boldsymbol{r}' \frac{\partial \Phi(\{n_\alpha\})}{\partial n_\alpha} \frac{\delta n_\alpha(\boldsymbol{r}')}{\delta \rho_i(\boldsymbol{r})}, \tag{8}$$

where Φ is the reduced free energy density and $\{n_\alpha\}$ are the set of weighted densities. The details about Φ and $\{n_\alpha\}$ are given in Ref. 40. The second term in Eq. (7) accounts for the fluid-fluid vdW attractive interactions using a mean field approximation.

B. Electrostatic potential

The electrostatic interactions, in addition to being long-ranged, also give rise to the short-range electrostatic correlations. The hard-sphere term, $U^{\text{ff}}_{i,\text{hs}}$, in Eq. (7) only accounts for the fluid-fluid short-range correlations due to the repulsive component of the vdW interactions. The short-range electrostatic correlations play an important role in determining the structure and electrostatic properties of EDLs. The short-range electrostatic correlation effects are especially dominant when the surface charge and/or the electrolyte concentration is high and the charge inversion occurs.[52]

In this work, we account for both the long-range mean electrostatic potential, $U_{i,\text{elec-mf}}(z)$, and short-range electrostatic correlation potential, $U_{i,\text{elec-corr}}(z)$, as

$$U_{i,\text{elec}}(z) = U_{i,\text{elec-mf}}(z) + U_{i,\text{elec-corr}}(z). \tag{9}$$

In Ref. 40, we present a Langevin-Poisson (LP) approach to compute the long-range electrostatic interactions. In the LP approach, a Poisson equation with spatially varying dielectric permittivity is solved to determine the mean electrostatic potential, ϕ, as

$$\frac{d}{dz}\left(\varepsilon_r(z)\frac{d\phi}{dz}\right) = -\frac{q_+\rho_+(z) + q_-\rho_-(z)}{\varepsilon_0}, \tag{10}$$

with boundary conditions

$$\left.\frac{d\phi}{dz}\right|_{z=0} = -\frac{\sigma_{\text{wall-L}}}{\varepsilon_0}, \tag{11a}$$

$$\left.\frac{d\phi}{dz}\right|_{z=L} = \frac{\sigma_{\text{wall-U}}}{\varepsilon_0}, \tag{11b}$$

$$\phi(z = L/2) = 0. \tag{11c}$$

In Eqs. (10) and (11), $\sigma_{\text{wall-L}}$ and $\sigma_{\text{wall-U}}$ are the surface charge densities of the lower ($z = 0$) and upper ($z = L$) walls, respectively, q_+ and q_- are the charges on the cation and anion, respectively, $\varepsilon_r(z)$ is the spatially dependent dielectric permittivity of water, and ε_0 is the vacuum dielectric constant. To obtain a non-trivial solution of the Poisson equation with the constant surface charge boundary conditions [Eq. (11a) and (11b)], we impose a zero potential condition at the mid-point of the channel via Eq. (11c). Therefore, $\phi(z)$ is the relative electrostatic potential with respect to the mid-point of the channel. A common approach in the theoretical treatment of the aqueous electrolytes is to assume $\varepsilon_r(z)$ to be constant and equivalent to the bulk dielectric permittivity of water. In Ref. 40, we model water molecules as point-like Langevin dipoles to include the effects of water orientation polarization and dielectric permittivity variation. The details of determining $\varepsilon_r(z)$ using the Langevin dipole model are given in Ref. 40.

The LP approach [Eq. (10)] is a mean-field approach, i.e., it ignores the short-range electrostatic correlations.

Therefore, $\phi(z)$ only accounts for the long-range mean electrostatic interactions. The mean-field electrostatic potential component, $U_{i,\text{elec-mf}}(z)$, for the ions and water molecules is determined as

$$U_{+/-,\text{elec-mf}}(z) = q_{+/-}\phi(z), \tag{12a}$$

$$U_{\text{w, elec-mf}}(z) = \mu\langle\cos\theta(z)\rangle\phi'(z), \tag{12b}$$

where $\phi'(z) = \frac{d\phi(z)}{dz}$, μ is the dipole moment of the water molecule, θ is the angle between the water dipole vector and the z-axis, and $\langle\cos\theta(z)\rangle$ is the average cosine of the dipole orientation. The details of determining $\langle\cos\theta(z)\rangle$ are given in Ref. 40.

In this work, we compute the electrostatic correlation contribution, $U_{i,\text{elec-corr}}$, to the electrostatic potential as

$$U_{i,\text{elec-corr}}(\boldsymbol{r}) = \sum_{j=1}^{3}\int_0^{R_{ij,\text{elec-corr}}} \rho_j(\boldsymbol{r}')u^{\text{ff}}_{ij,\text{elec-corr}}(r)d\boldsymbol{r}', \tag{13}$$

where $u^{\text{ff}}_{ij,\text{elec-corr}}(r)$ is the electrostatic correlation component of the fluid-fluid interaction between the fluid molecules i and j and $R_{ij,\text{elec-corr}}$ defines the range for the electrostatic correlations. We estimate the electrostatic correlation component of the fluid-fluid interaction, $u^{\text{ff}}_{ij,\text{elec-corr}}(r)$, from a bulk residual direct correlation function, $\Delta c_{ij}(r)$, as

$$u^{\text{ff}}_{ij,\text{elec-corr}}(r) = -k_{\text{B}}T\Delta c_{ij}(r). \tag{14}$$

The residual direct correlation function is due to the short-range component of the Coulombic interactions and is defined as[53,54]

$$\Delta c_{ij}(r) = c_{ij}(r) - c_{ij,\text{hs}}(r) + \frac{1}{k_{\text{B}}T}u_{ij,\text{vdw}}(r)\mathcal{H}\left(r - d_{ij,\text{hs}}\right) + \frac{1}{k_{\text{B}}T}\frac{q_iq_j}{4\pi\varepsilon_0\varepsilon_{\text{r}}r}, \tag{15}$$

where $c_{ij}(r)$ is the direct correlation function and $c_{ij,\text{hs}}(r)$ is the hard-sphere component of the direct correlation function between fluid particles i and j in the bulk electrolyte system. In Eq. (15), the third term is the component of the direct correlation due to fluid-fluid vdW attractive interactions in a mean field approximation, $\mathcal{H}$ is a Heaviside step function, $d_{ij,\text{hs}} = \frac{d_{i,\text{hs}}+d_{j,\text{hs}}}{2}$ is the effective hard sphere diameter for the fluid pair $i-j$, and the fourth term is due to the mean-field Coulomb interaction. We obtain $c_{ij}(r)$ from the solution of the Ornstein-Zernike (OZ) equation with the hypernetted chain (HNC) closure relation.[55]

III. CHARGE INVERSION SYSTEM

To demonstrate EQT for a charge inversion system, we simulate a KCl aqueous electrolyte confined inside a slit-like graphene channel. The electrolyte fluid is confined between two parallel, uniformly, and negatively charged graphene walls with -0.2265 C/m^2 surface charge density and 3.804 nm channel width. The confined electrolyte is assumed to be in thermodynamic equilibrium with a reference bulk electrolyte system with 1.0 M bulk ion concentration in water at 1.0 g/cm^3 density and 298 K temperature. To check the accuracy of EQT, we compare the EQT results with MD simulations.

The reference MD simulations are performed in the NVT (canonical) ensemble by GROMACS.[56] Two graphene walls are placed along the xy plane and the lateral dimensions of the walls are 3.834×3.68927 nm^2. The wall atoms are kept fixed. To achieve the surface charge density of -0.2265 C/m^2, a uniform partial charge of -0.037 e is assigned to the wall atoms. Periodic boundary conditions are used in the x, y, and z directions. Water is modeled using the SPC/E (extended simple point charge model)[57] force field and ions are modeled using the force field of Joung and Cheatham.[58] A spherical cutoff of 0.9 nm is used for the LJ interactions, and electrostatic interactions are computed by the particle-mesh Ewald (PME) technique.[59] The simulation box is padded with a vacuum layer of $50\sigma_{\text{ow}}$ in the z dimension along with a correction for the slab geometry to exclude the interactions between the periodic images in z. Temperature is maintained using the Nosé-Hoover thermostat[60] with 0.5 ps time constant. Equations of motion are integrated with the leap-frog algorithm with a time step of 1 fs. For a given bulk ion concentration and surface charge density, the number of ions and water molecules is determined by a trial-and-error approach such that the bulk fluid densities are achieved in the center of the channel. The number of fluid molecules used in the AA-MD simulations is: 1640 water molecules, 77 K^+ ions, and 37 Cl^- ions. Equilibrium properties are obtained by averaging the values from 10 ns long trajectories.

Figure 1 shows the density profiles of K^+, Cl^-, and water center of mass (COM) obtained from MD simulations. Since the surface charge is negative, in this case, K^+ ions are counterions and Cl^- are coions. As expected, water molecules arrange in distinct layers near the channel walls. We observe that majority of K^+ ions accumulate within 0.4 nm distance from the

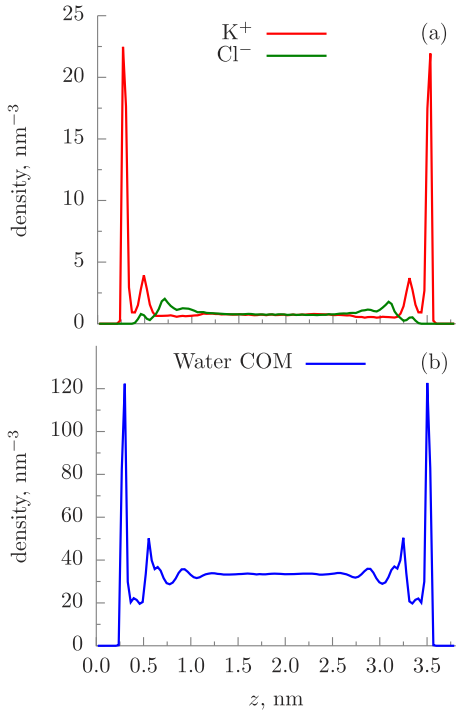

FIG. 1. Ion (a) and water COM (b) density profiles from the reference AA-MD simulations of the charge inversion phenomenon in KCl aqueous electrolyte confined inside a slit-like graphene channel.

walls, Cl^- ion density is very low within 0.4 nm distance from the walls, and Cl^- (coion) density is higher than the density of K^+ (counterion) between 0.6 and 1.4 nm distance from the walls. Therefore, the charge inversion occurs at 0.6 nm distance away from the walls.

IV. COARSE-GRAINED (CG) POTENTIALS

In EQT, to compute $U^{\mathrm{wf}}_{i,\mathrm{vdw}}$, $U^{\mathrm{ff}}_{i,\mathrm{vdw}}$, and $\Delta c_{ij}(r)$, we need to specify $u^{\mathrm{wf}}_i(r)$ and $u^{\mathrm{ff}}_{ij,\mathrm{vdw}}(r)$. In Eqs. (6), (7), and (15), $u^{\mathrm{wf}}_i(r)$ and $u^{\mathrm{ff}}_{ij,\mathrm{vdw}}(r)$ are assumed to be spherically symmetric isotropic pair potentials. Classical atomistic force fields, which are used in MD simulations, provide vdW pair potentials for wall-fluid and fluid-fluid interactions. In the atomistic force fields, vdW interactions of ions are commonly modeled with the pair additive potentials. For monoatomic ions, the ion-ion and ion-wall potentials are spherically symmetric and, hence, they are straightforward to use in Eqs. (6), (7), and (15). However, in MD, the water molecule is modeled with the three sites SPC/E model to represent hydrogen and oxygen atoms and partial charge distribution. Due to multiple sites per water molecule, the water-water and ion-water interactions in an atomistic force field are anisotropic, i.e., they depend not only on the separation distance between molecules but also on the relative orientation. Therefore, it is more complex to use a fully atomistic force field of water in a continuum framework. Hence, we need a simple yet accurate potential model for water which can incorporate the effects of water polarization and ion-water interactions. Therefore, we first develop a coarse-grained water force field and single site spherically symmetric ion-water coarse-grained potentials as described in the following.

We follow a systematic coarse-graining approach to develop a CG model of the confined KCl electrolyte charge inversion system. Systematic coarse-graining is a bottom-up approach to devise CG models by systematically linking a low resolution CG system to a reference high resolution all atom (AA) system.[61–63] In this work, we first obtain the CG potentials in the particle based CG MD framework and use the same CG interactions in EQT.

We explore two coarse-grained representations for the water molecule: (i) single coarse-grained bead at the center of mass (COM) with zero charge and no dipole moment, denoted as (oW) CG water model, and (ii) point dipole model, denoted as (μW) CG water model. oW CG water is a single site isotropic model that is easy to incorporate accurately in a continuum-based approach like EQT. However, the oW CG model cannot explicitly model water polarization effects and screening of electrostatic interactions in ionic systems. On the other hand, μW CG water can model the effects of water polarization and permittivity variation in EDL. However, due to orientation dependence and anisotropic nature of dipole-dipole and ion-dipole electrostatic interactions, μW CG water is challenging to model accurately in a continuum-based approach.

We use the relative entropy minimization method[64,65] to coarse-grain the confined KCl system. Detailed description of the relative entropy-based coarse-graining of the aqueous electrolyte systems and point dipole water model is given in Ref. 40. Relative entropy minimization is performed using the versatile object-oriented toolkit for coarse-graining applications (VOTCA).[66,67] In both, oW and μW, CG models, the ion-ion vdW interactions are the same as the LJ interactions in the atomistic force-field. The charges on the ions are also kept the same as in the atomistic force field. As discussed in Ref. 40, due to anisotropic and inhomogeneous interfacial arrangement of the water molecules and ions, the bulk-based water-water and ion-water CG potentials are not exact near the surface. Therefore, as suggested in Refs. 44 and 45, we also coarse-grain wall-water and wall-ion interactions to account for the errors arising from the bulk-based CG potentials near the interface.

A. *o*W CG water

In the oW water based CG representation of the KCl electrolyte system, we assume a uniform permittivity of 78.5 to incorporate screening effects of water. For the water-water interaction, we use the water-water CG potential obtained from bulk water in Ref. 67. K^+-water and Cl^--water CG potentials are determined from the bulk KCl electrolyte system by relative entropy minimization. Wall-water and wall-ion interactions are optimized by relative entropy based coarse-graining of the confined KCl electrolyte system. Figure 2 shows the water-water, ion-water, wall-water, and wall-ion CG potentials. From Fig. 3, we observe that the CG potentials can accurately predict the water and ion density profiles by CG MD simulations. This suggests that, though oW CG water representation assumes a uniform permittivity, the effects of water polarization and permittivity variations in the double layer region near the charged surface are accurately incorporated in the wall-water and wall-ion CG potentials.

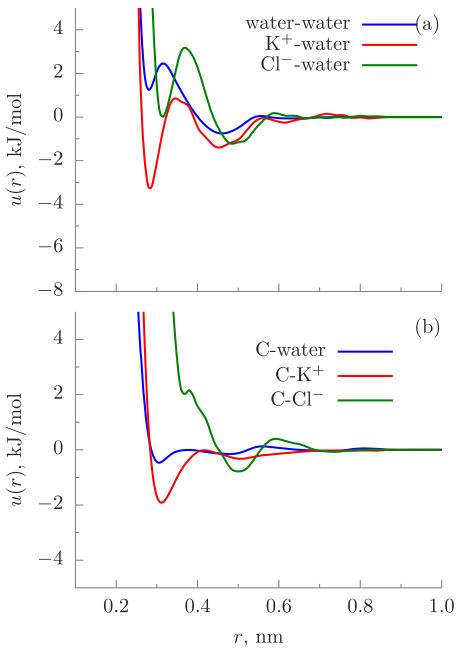

FIG. 2. CG potentials in the oW water based CG representation of the KCl electrolyte system: (a) Water-water, K^+-water, and Cl^--water CG potentials and (b) C-water, C–K^+, and C–Cl^- CG potentials.

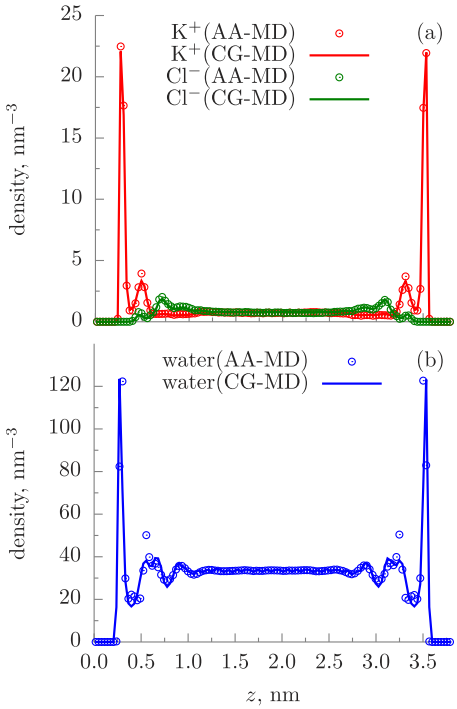

FIG. 3. Comparison of ion density profiles (a) and water COM density profiles (b) from AA-MD and CG-MD with oW water based CG potentials of the confined KCl electrolyte system.

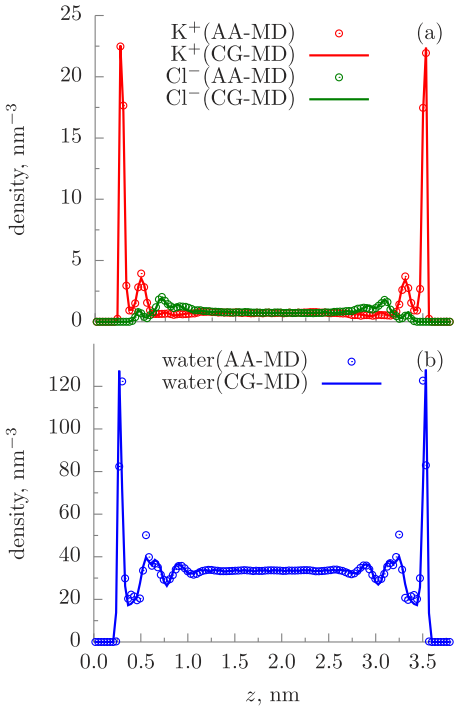

FIG. 5. Comparison of ion density profiles (a) and water COM density profiles (b) from AA-MD and CG-MD with μW water based CG potentials of the confined KCl electrolyte system.

B. μW CG water

In the μW water based CG representation, we use the same water-water CG potential obtained in Ref. 40 with $\mu = 2.88$ D which reproduces both the radial distribution function (RDF) and permittivity of bulk water. K^+-water and Cl^--water CG potentials are determined from the bulk KCl electrolyte system by relative entropy minimization. Wall-water and wall-ion interactions are optimized by relative entropy based coarse-graining of the confined KCl electrolyte system. Figure 4 shows the water-water, ion-water, wall-water, and wall-ion CG potentials. From Fig. 5, we observe that the CG potentials can accurately predict the water and ion density profiles by CG MD simulations. We note that, unlike in the oW water based CG representation of the confined KCl electrolyte system, in μW representation we do not assume a uniform permittivity.

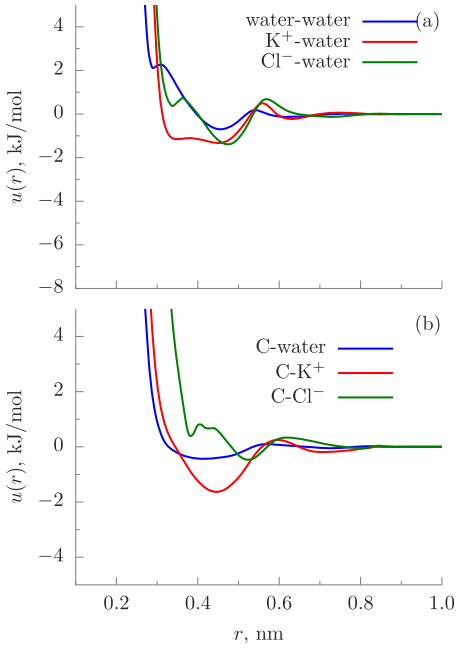

FIG. 4. CG potentials in the μW water based CG representation of the KCl electrolyte system: (a) Water-water, K^+-water, and Cl^--water CG potentials and (b) C-water, C–K^+, and C–Cl^- CG potentials.

V. RESULTS

A. Limitations of Langevin-Poisson mean-field electrostatics

First, we test the ability of the LP-EQT framework with mean-field electrostatics, and no electrostatic correlations, to predict the charge inversion phenomenon in the confined KCl electrolyte system. For this test, we use the μW CG water model. For LP-EQT simulations, we follow the same procedure as described in detail in Ref. 40. In EQT, we solve Eqs. (3)–(7) self-consistently to determine density and potential profiles of ions and water. The reference densities and potentials required in Eq. (3) are determined from the reference bulk system. The reference bulk potentials, $U_{i,\mathrm{ref}}$, are computed by substituting the bulk densities in Eq. (7). To compute the attractive part of the vdW potential from Eq. (7), we use the CG pair potentials, i.e.,

$$u_{ij}^{\mathrm{ff}}(r) = u_{ij,\mathrm{cg}}^{\mathrm{ff}}(r), \tag{16}$$

where $u_{ij,\mathrm{cg}}^{\mathrm{ff}}$ is the CG interaction between the molecules i and j. The ion-ion pairs, $u_{ij,\mathrm{cg}}^{\mathrm{ff}}$, are the same LJ potentials as

in the reference MD simulations (see Sec. III), and for the water-water and ion-water pairs, we use the CG pair potentials obtained in Sec. IV. For all the pair potentials, we set $R^{\text{ff}}_{ij,\text{cut}} = 0.9$ nm. We set $R^{\text{ff}}_{ij,\text{min}} = \sigma^{\text{ff}}_{ij}$ for the ion-ion LJ pair potentials, where σ^{ff}_{ij} is the usual LJ parameter. For the water-water and ion-water CG potentials, we set $R^{\text{ff}}_{ij,\text{min}}$ to be the location of the first minima of the corresponding CG pair potential. Therefore, $R^{\text{ff}}_{\text{ww, min}} = 0.28$ nm, $R^{\text{ff}}_{\text{+w, min}} = 0.263$ nm, and $R^{\text{ff}}_{\text{−w, min}} = 0.314$ nm. To compute the wall-fluid potential energies from Eq. (6), we use $\rho_{\text{wall}} = 38.18$ atoms/nm^3 for the graphene walls. For the wall-water and wall-ion interactions, we use the same LJ pair potential as that in the reference MD simulations. To determine the mean electrostatic potential, $\phi(z)$, we solve Eqs. (10) and (11) with $q_+ = +1.0$ e and $q_- = -1.0$ e and $\mu = 2.88$ D. Both the channel walls are negatively charged such that $\sigma_{\text{wall-L}} = \sigma_{\text{wall-U}} = -0.2265$ C/m^2. To determine the hard-sphere energy component from FMT [Eq. (8)], we use $d_{\text{hs,w}} = 0.28$ nm, $d_{\text{hs,+}} = 0.18$ nm, and $d_{\text{hs,−}} = 0.23$ nm. The numerical solution approach to self-consistently solve Eqs. (3)–(7) is described in Ref. 40.

Figure 6 shows the comparison of the water and ion density profiles for the confined KCl electrolyte system from the LP-EQT and AA MD simulations. We observe that the water density profile from the LP-EQT compares well with reference MD simulations. However, the LP-EQT framework fails to accurately predict ion density profiles and the charge inversion phenomenon near the walls. The errors in the LP-EQT results can be attributed to the simplifications and approximations made in the LP-EQT framework. The Langevin-Poisson (LP) model is a mean-field approach and, hence, it ignores ion-ion, ion-dipole, and dipole-dipole short-range electrostatic correlations.[34] In addition, the LP model neglects higher electric moments of the water molecule, such as a quadrupole moment, which also contribute to the dielectric permittivity variation of confined water.[68,69] Also, for the water-water and ion-water interactions, we use the CG potentials determined from the bulk systems. Since the interfacial arrangement of the water molecules and ions is different from the bulk, the bulk-based CG potentials are not exact near the surface. Therefore, as described in Secs. II and IV, we extend the LP-EQT framework to include short-range electrostatic correlations and accurate wall-water and wall-ion CG potentials obtained in Sec. IV. The results of the modified LP-EQT framework with the electrostatic correlations and wall-fluid CG potentials are presented in Subsections V B and V C.

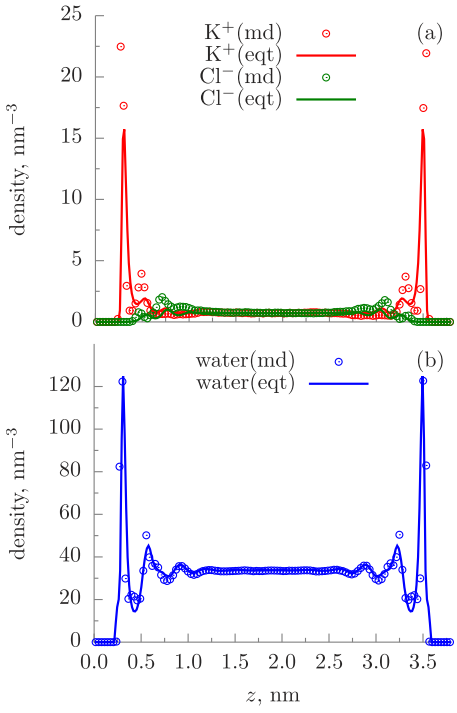

FIG. 6. Comparison of ion density profiles (a) and water COM density profiles (b) from AA MD and LP-EQT for the charge inversion phenomenon in the confined KCl electrolyte system.

B. Electrostatic correlations

In this section, we determine the ion-ion short-range electrostatic correlations for both the oW and μW CG water models. As described in Sec. II B, we model ion-ion short-range electrostatic correlations as the residual direct correlation function, $\Delta c_{ij}(r)$, defined by Eq. (15). To compute $\Delta c_{ij}(r)$ from Eq. (15), we need $c_{ij}(r)$, $c_{ij,\text{hs}}(r)$, and $u_{ij,\text{vdw}}(r)$. For $u_{ij,\text{vdw}}(r)$, we use the CG potentials. $c_{ij}(r)$ is obtained from the solution of the Ornstein-Zernike (OZ) equation with the hypernetted chain (HNC) closure and CG potential model for the bulk electrolyte. Similarly, $c_{ij,\text{hs}}(r)$ is determined from the HNC solution of the OZ equation with the hard-sphere pair potentials. We note that, in Eq. (15), the attractive part of the vdW pair potential and long range electrostatics are treated in the mean-field sense and the range, $R_{ij,\text{elec-corr}}$, of the residual correlations due to the short-range electrostatic interactions is similar to the hard-sphere diameter, $d_{ij,\text{hs}}$.[53,54]

1. oW CG water

Figure 7 shows the ion-ion residual direct correlation functions for the CG bulk 1 M KCl electrolyte system with the oW CG water model and uniform permittivity of $\varepsilon_r = 78.5$. To compute $c_{ij,\text{hs}}(r)$, we use the hard-sphere diameters of 0.28, 0.18, and 0.32 nm for the water CG bead, K$^+$, and Cl$^-$, respectively. We also verify the ion-water RDFs computed from the HNC-based solution of the OZ equation using oW water CG potentials. Figure 8 shows that the RDFs from HNC with the ion-water CG potentials compare well with the

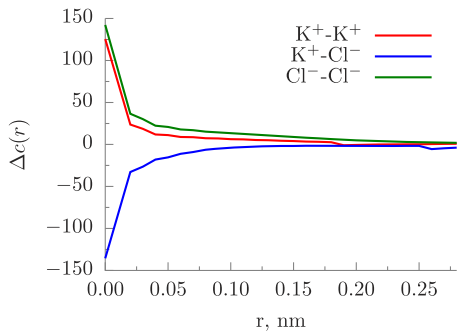

FIG. 7. Residual direct correlations for the CG bulk 1M KCl electrolyte system using the oW CG water model.

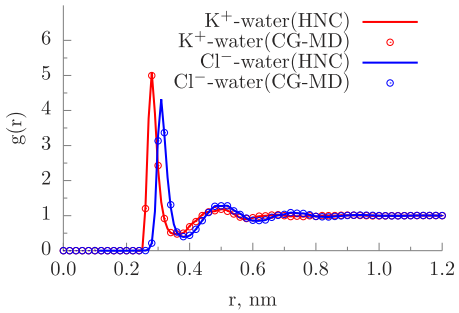

FIG. 8. Comparison of ion-water RDFs from CG-MD and HNC using oW CG water potentials.

CG-MD RDFs. This suggests that HNC with the CG potentials can reliably predict the correlations in the bulk electrolyte system.

2. μW CG water

Equations (13) and (14) assume the fluid-fluid electrostatic correlations are spherically symmetric. However, in the case of a point-dipole CG water model, μW, dipole-dipole, and ion-dipole correlations are orientation dependent. Here, for numerical simplicity, we ignore dipole-dipole electrostatic correlations and incorporate the effects of ion-dipole correlations into an effective spherically symmetric ion-ion correlations defined as[70,71]

$$c_{ij}^{\text{eff}}(r) = c_{ij}^{000}(r) + \rho_{\text{w}} \frac{c_{i-\text{w}}^{000}(r) c_{j-\text{w}}^{000}(r)}{1 - \rho_{\text{w}} c_{\text{w-w}}^{000}(r)} - \frac{1}{3}\rho_{\text{w}} \frac{c_{i-\text{w}}^{011}(r) c_{j-\text{w}}^{011}(r)}{1 - \rho_{\text{w}}\left(c_{\text{w-w}}^{110}(r) + 2c_{\text{w-w}}^{112}(r)\right)}, \quad (17)$$

where $c_{\alpha\beta}^{mnl}(r)$ are the projections of the direction correlation between fluid particles α and β in the rotational invariant based expansion.[71] We obtain $c_{\alpha\beta}^{mnl}(r)$ from the linearized hypernetted-chain (LHNC)[71,72] approximation based solution of the OZ equation in the bulk electrolyte system. To solve the OZ equation with LHNC approximation, we follow the numerical scheme of Levesque *et al.*[71] Then, the effective correlations, $c_{ij}^{\text{eff}}(r)$, can be substituted for $c_{ij}(r)$ in Eq. (15) to obtain the ion-ion residual correlation for the μW CG water based electrolyte system.

Figure 9 shows the ion-ion residual direct correlation functions for the CG bulk 1 M KCl electrolyte system with

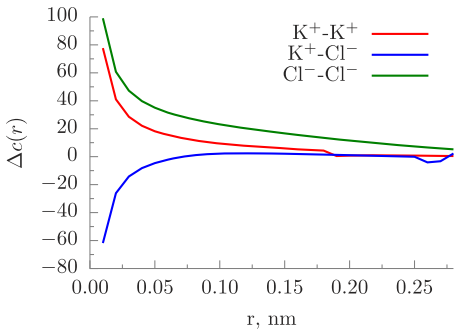

FIG. 9. Ion-ion residual direct correlations for the CG bulk 1M KCl electrolyte system using the μW CG water model.

the μW CG water model. To compute $c_{ij,\text{hs}}(r)$, we use the hard-sphere diameters of 0.28, 0.18, and 0.32 nm for the water CG bead, K^+, and Cl^-, respectively. We also verify projections of the ion-water total correlations, $h_{i-\text{w}}^{mnl}(r)$, computed from the LHNC-based solution of the OZ equation using μW water CG potentials. Figure 10 shows that $h_{i-\text{w}}^{mnl}(r)$ from LHNC with the ion-dipole CG potentials compare well with the CG-MD results.

C. EQT with electrostatic correlations

1. oW CG water

First, we use the oW water based CG model of the confined KCl electrolyte system in EQT to obtain ion and water density profiles. For the ion-ion interactions, we use the same LJ potentials that are used in the reference MD simulations. For the water-water, ion-water, wall-water, and wall-ion pair interactions, we use the systematically developed CG potentials discussed in Sec. IV. For all the pair potentials, we set $R_{ij,\text{cut}}^{\text{ff}} = 0.9$ nm. Here, we set $R_{ij,\text{min}}^{\text{ff}} = \sigma_{ij}^{\text{ff}}$ for the ion-ion LJ pair potentials, where σ_{ij}^{ff} is the usual LJ parameter. For the water-water and ion-water CG potentials, we set $R_{\text{ww, min}}^{\text{ff}} = 0.28$ nm, $R_{\text{+w, min}}^{\text{ff}} = 0.262$ nm, and $R_{\text{−w, min}}^{\text{ff}} = 0.314$ nm. To compute the wall-fluid potential energies from Eq. (6), we use $\rho_{\text{wall}} = 38.18$ atoms/nm^3 for the graphene walls. To determine the mean electrostatic potential, $\phi(z)$, we solve Eqs. (10) and (11) with $q_+ = +1.0$ e and $q_- = -1.0$ e and a uniform permittivity of $\varepsilon_{\text{r}} = 78.5$. The walls are equally charged such that $\sigma_{\text{wall-L}} = \sigma_{\text{wall-U}} = \sigma_{\text{wall}}$, where $\sigma_{\text{wall}} = -0.2265$ C/m^2. To determine the hard-sphere energy component from FMT [Eq. (8)], we use $d_{\text{hs,w}} = 0.28$ nm, $d_{\text{hs,+}} = 0.18$ nm, and $d_{\text{hs,−}} = 0.32$ nm. In addition, here, we also include the electrostatic correlations determined from Eq. (13) with the residual correlations shown in Fig. 7.

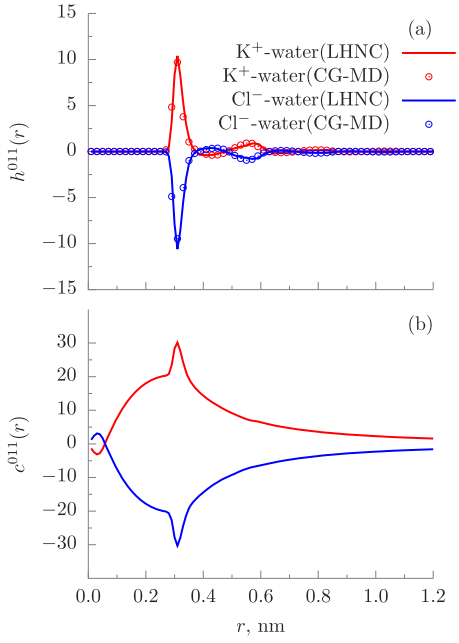

FIG. 10. (a) Comparison of ion-water total correlation $h^{011}(r)$ projections from CG-MD and LHNC for the CG bulk 1M KCl electrolyte using the μW CG water model. (b) Ion-water direct correlation $c^{011}(r)$ projections.

Figure 11 shows the comparison of the density profiles from EQT and MD for water and ions. It can be seen that the water and ion density profiles from EQT compare well with the reference MD simulations. We show that the systematically obtained CG potentials and inclusion of electrostatic correlations improve the accuracy of EQT so that it can predict the charge inversion phenomenon well compared with the reference AA MD simulations.

2. μW CG water

The main advantage of the μW CG water model is that it can explicitly incorporate the spatially varying nature of the dielectric permittivity and the orientation polarization of water molecules near charged surfaces. Therefore, for μW CG water based EQT simulations of the confined KCl electrolyte system, we use the Langevin dipole based computation of the mean-field electrostatic potential as described in Sec. II B. In addition to the mean-field electrostatic potential, we include the ion-ion electrostatic correlations determined from Eq. (13) with the effective ion-ion residual correlations shown in Fig. 9. The remaining EQT simulation parameters are as follows.

For the ion-ion interactions, we use the same LJ potentials that are used in the reference MD simulations. For the water-water, ion-water, wall-water, and wall-ion pair interactions, we use the systematically developed CG potentials with the μW CG water model as discussed in Sec. IV. For all the pair potentials, we set $R^{\text{ff}}_{ij,\text{cut}} = 0.9$ nm. Here, we set $R^{\text{ff}}_{ij,\text{min}} = \sigma^{\text{ff}}_{ij}$ for the ion-ion LJ pair potentials, where σ^{ff}_{ij} is the usual LJ parameter. For the water-water and ion-water CG potentials, we set $R^{\text{ff}}_{\text{ww, min}} = 0.28$ nm, $R^{\text{ff}}_{\text{+w, min}} = 0.32$ nm, and $R^{\text{ff}}_{\text{−w, min}} = 0.338$ nm. To compute the wall-fluid potential energies from Eq. (6), we use $\rho_{\text{wall}} = 38.18$ atoms/nm^3 for the graphene walls. To determine the mean electrostatic potential, $\phi(z)$, we solve Eqs. (10) and (11) with $q_+ = +1.0$ e, $q_- = -1.0$ e, $\mu = 3.84$ D, and spatially varying permittivity. The walls are equally charged such that $\sigma_{\text{wall-L}} = \sigma_{\text{wall-U}} = \sigma_{\text{wall}}$, where $\sigma_{\text{wall}} = -0.2265$ C/m^2. To determine the hard-sphere energy component from FMT [Eq. (8)], we use $d_{\text{hs,w}} = 0.28$ nm, $d_{\text{hs,+}} = 0.18$ nm, and $d_{\text{hs,−}} = 0.32$ nm.

Figure 12 shows the density profiles from EQT with the μW CG water model. We observe that the EQT with the μW CG water model and ion-ion effective electrostatic correlations fail to capture density profiles of ions accurately. The errors in the predictions of EQT can be attributed to the bulk-based approximation used to determine the ion-ion effective correlations from Eq. (17). We note that the ion-ion effective correlations depend on the ion-dipole correlations. It is known that near an interface, the dipole orientation of water is widely different from that of the bulk water.[73] Therefore, the bulk-based ion-dipole correlations, which are used in Eq. (17), may not be accurate near the charged interface of EDL.

One approach to account for the orientation polarization effects of water dipoles on the ion densities near the interface is to obtain an effective wall-ion CG potential in EQT. We followed the similar approach for the NaCl electrolyte confined inside capacitor channels as in Ref. 40. We note that the wall-fluid CG potentials obtained in the CG-MD with the oW CG water model account for the orientation polarization effects of SPC/E water on the ion densities. Therefore, here, to incorporate the interfacial orientation polarization

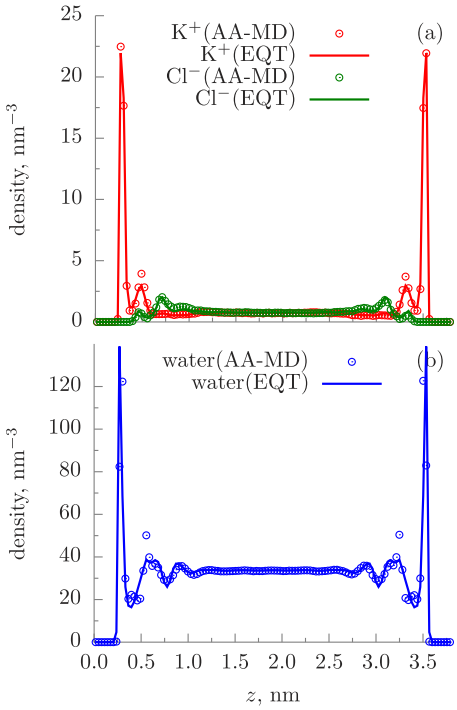

FIG. 11. Comparison of ion density profiles (a) and water COM density profiles (b) from AA MD and EQT with oW water based CG potentials of the confined KCl electrolyte system.

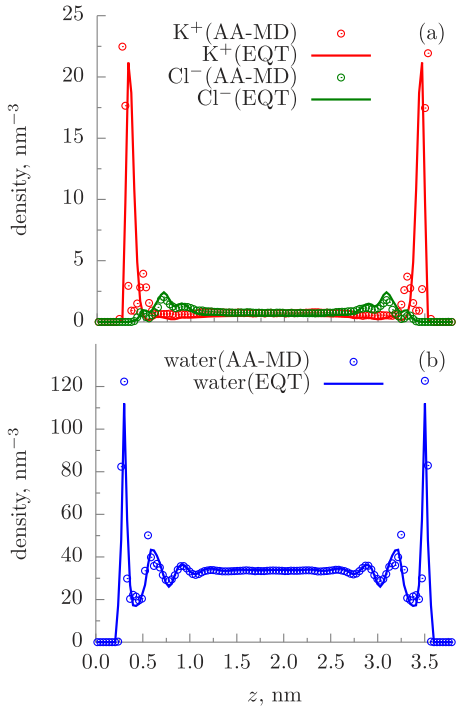

FIG. 12. Comparison of ion density profiles (a) and water COM density profiles (b) from AA MD and EQT with μW water based CG potentials of the confined KCl electrolyte system.

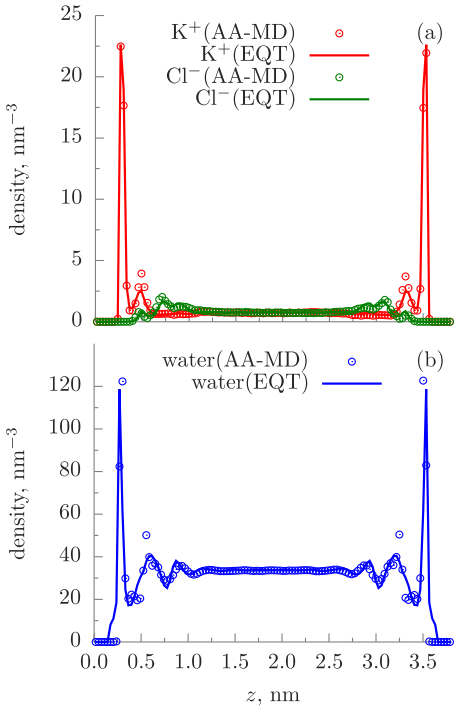

FIG. 13. Comparison of ion density profiles (a) and water COM density profiles (b) from AA MD and EQT with the μW water model and modified wall-water and wall-K^+ CG potentials in EQT.

effects of water on K^+ density, we use the same C-water and C-K^+ CG potentials obtained with the oW CG model in CG-MD (see Fig. 2). For the wall-Cl^-, water-water, K^+-water, and Cl^--water, we use the μW water model based CG potentials. We also include the bulk-based ion-ion effective electrostatic residual correlations. Figure 13 shows the comparison of the density profiles from EQT and MD for water and ions. It can be seen that, with appropriate wall-fluid CG potentials and ion-ion residual correlations from the bulk, the water and ion density profiles from EQT with the μW CG water model compare well with the reference MD simulations.

VI. CONCLUSIONS

In this paper, we extended the LP-EQT framework to predict the charge inversion phenomenon in EDLs. We found that the ion-ion and ion-dipole electrostatic correlations are important for the charge inversion. We modeled the electrostatic correlations using the residual direct correlation functions of the bulk electrolyte. The bulk residual direct correlation functions are determined from the HNC-based integral equation theory. We explored two coarse-grained representations for the water molecule: oW CG water with no dipole and μW CG water with point dipole. We showed that, with the systematically obtained CG potentials and the inclusion of electrostatic correlations, EQT can predict the charge inversion phenomenon well compared to MD simulations.

ACKNOWLEDGMENTS

This work was supported by NSF under Grant Nos. 1420882, 1506619, 1720701, 1720633, and 1545907.

[1]K. Besteman, K. Van Eijk, and S. G. Lemay, Nat. Phys. **3**, 641 (2007).
[2]I. Rouzina and V. A. Bloomfield, J. Phys. Chem. **100**, 9977 (1996).
[3]M. Lozada-Cassou, Phys. Rev. E **60**, R17 (1999).
[4]M. Quesada-Prez, E. Gonzlez-Tovar, A. Martn-Molina, M. Lozada-Cassou, and R. Hidalgo-lvarez, ChemPhysChem **4**, 234 (2003).
[5]R. Qiao and N. R. Aluru, Phys. Rev. Lett. **92**, 198301 (2004).
[6]P. S. Kuhn, Y. Levin, and M. C. Barbosa, Phys. A: Stat. Mech. Appl. **274**, 8 (1999).
[7]Y. He, D. Gillespie, D. Boda, I. Vlassiouk, R. S. Eisenberg, and Z. S. Siwy, J. Am. Chem. Soc. **131**, 5194 (2009).
[8]M. A. Shannon, P. W. Bohn, M. Elimelech, J. G. Georgiadis, B. J. Marias, and A. M. Mayes, Nature **452**, 301 (2008).
[9]M. Heiranian, A. B. Farimani, and N. R. Aluru, Nat. Commun. **6**, 8616 (2015).
[10]B. E. Conway, *Electrochemical Supercapacitors Scientific Fundamentals and Technological Applications* (Springer US, Boston, MA, 1999), ISBN: 978-1-4757-3058-6.
[11]P. Simon and Y. Gogotsi, Nat. Mater. **7**, 845 (2008).
[12]L. Bocquet and E. Charlaix, Chem. Soc. Rev. **39**, 1073 (2010).
[13]F. Zaera, Surf. Sci. **605**, 1141 (2011).
[14]F. Zaera, Chem. Rev. **112**, 2920 (2012).
[15]O. Björneholm, M. H. Hansen, A. Hodgson, L.-M. Liu, D. T. Limmer, A. Michaelides, P. Pedevilla, J. Rossmeisl, H. Shen, G. Tocci *et al.*, Chem. Rev. **116**, 7698 (2016).
[16]M. P. Allen and D. J. Tildesley, *Computer Simulation of Liquids* (Oxford University Press, 1989), ISBN: 978-0-19-855645-9.
[17]D. Frenkel and B. Smit, *Understanding Molecular Simulation: From Algorithms to Applications* (Academic Press, 2001), ISBN: 978-0-08-051998-2.
[18]R. Qiao and N. R. Aluru, J. Chem. Phys. **118**, 4692 (2003).
[19]P. Wu and R. Qiao, Phys. Fluids **23**, 072005 (2011).
[20]S. Attinger and P. Koumoutsakos, *Multiscale Modeling and Simulation* (Springer, New York, 2004).
[21]H.-J. Butt, K. Graf, and M. Kappl, *Physics and Chemistry of Interfaces* (Wiley-VCH Verlag GmbH & Co. KGaA, 2003), pp. 42–56, ISBN: 978-3-527-60231-5.
[22]I. Borukhov, D. Andelman, and H. Orland, Phys. Rev. Lett. **79**, 435 (1997).
[23]R. Kjellander, T. Kesson, B. Jnsson, and S. Marelja, J. Chem. Phys. **97**, 1424 (1992).
[24]R. Evans and T. J. Sluckin, Mol. Phys. **40**, 413 (1980).
[25]J. Wu, AIChE J. **52**, 1169 (2006).
[26]J. W. Lee, R. H. Nilson, J. A. Templeton, S. K. Griffiths, A. Kung, and B. M. Wong, J. Chem. Theory Comput. **8**, 2012 (2012).
[27]A. L. Frischknecht, D. O. Halligan, and M. L. Parks, J. Chem. Phys. **141**, 054708 (2014).
[28]J. W. Lee, A. Mani, and J. A. Templeton, Langmuir **31**, 7496 (2015).
[29]K. M. Salerno, A. L. Frischknecht, and M. J. Stevens, J. Phys. Chem. B **120**, 5927 (2016).
[30]*Fundamentals of Interface and Colloid Science*, Volume 2 of Solid-Liquid Interfaces, edited by J. Lyklema (Academic Press, 1995), p. 3-1.
[31]M. F. Chaplin, in *Adsorption and Phase Behaviour in Nanochannels and Nanotubes*, edited by P. L. J. Dunne and D. G. Manos (Springer Netherlands, 2010), pp. 241–255.
[32]S. Lamperski and A. Zydor, Electrochim. Acta **52**, 2429 (2007).
[33]T. Goel, C. N. Patra, S. K. Ghosh, and T. Mukherjee, J. Chem. Phys. **129**, 154906 (2008).
[34]E. Gongadze, A. Velikonja, S. Perutkova, P. Kramar, A. Maek-Lebar, V. Kralj-Igli, and A. Igli, Electrochim. Acta **126**, 42 (2014).
[35]E. Gongadze and A. Igli, Electrochim. Acta **178**, 541 (2015).
[36]A. Oleksy and J.-P. Hansen, J. Chem. Phys. **132**, 204702 (2010).
[37]T. Biben, J. P. Hansen, and Y. Rosenfeld, Phys. Rev. E **57**, R3727 (1998).
[38]V. Warshavsky and M. Marucho, Phys. Rev. E **93**, 042607 (2016).
[39]D. Henderson, D.-e. Jiang, Z. Jin, and J. Wu, J. Phys. Chem. B **116**, 11356 (2012).
[40]S. Y. Mashayak and N. R. Aluru, J. Chem. Phys. **146**, 044108 (2017).
[41]A. V. Raghunathan, J. H. Park, and N. R. Aluru, J. Chem. Phys. **127**, 174701 (2007).
[42]T. Sanghi and N. R. Aluru, J. Chem. Phys. **132**, 044703 (2010).
[43]T. Sanghi and N. R. Aluru, J. Chem. Phys. **136**, 024102 (2012).
[44]S. Y. Mashayak and N. R. Aluru, J. Chem. Theory Comput. **8**, 1828 (2012).
[45]S. Y. Mashayak and N. R. Aluru, J. Chem. Phys. **137**, 214707 (2012).
[46]S. Y. Mashayak, M. H. Motevaselian, and N. R. Aluru, J. Chem. Phys. **142**, 244116 (2015).

[47]M. H. Motevaselian, S. Y. Mashayak, and N. R. Aluru, J. Chem. Phys. **143**, 124106 (2015).
[48]M. H. Motevaselian and N. R. Aluru, J. Chem. Phys. **146**, 154102 (2017).
[49]A. Y. Grosberg, T. T. Nguyen, and B. I. Shklovskii, Rev. Mod. Phys. **74**, 329 (2002).
[50]J. Lyklema, Colloids Surf., A **291**, 3 (2006).
[51]R. Roth, J. Phys.: Condens. Matter **22**, 063102 (2010).
[52]E. Wernersson, R. Kjellander, and J. Lyklema, J. Phys. Chem. C **114**, 1849 (2010).
[53]Z. Tang, L. E. Scriven, and H. T. Davis, J. Chem. Phys. **97**, 9258 (1992).
[54]J.-P. Hansen and I. R. McDonald, *Theory of Simple Liquids* (Elsevier, 2013), pp. 403–454.
[55]J.-P. Hansen and I. R. McDonald, in *Theory of Simple Liquids*, 4th ed., edited by J.-P. Hansen and I. R. McDonald (Academic Press, Oxford, 2013), pp. 105–147.
[56]S. Pronk, S. Páll, R. Schulz, P. Larsson, P. Bjelkmar, R. Apostolov, M. R. Shirts, J. C. Smith, P. M. Kasson, D. van der Spoel *et al.*, Bioinformatics **29**, 845 (2013).
[57]H. J. C. Berendsen, J. R. Grigera, and T. P. Straatsma, J. Phys. Chem. **91**, 6269 (1987).
[58]I. S. Joung and T. E. Cheatham, J. Phys. Chem. B **112**, 9020 (2008).
[59]T. Darden, D. York, and L. Pedersen, J. Chem. Phys. **98**, 10089 (1993).
[60]S. Nosé, J. Chem. Phys. **81**, 511 (1984).
[61]C. Peter and K. Kremer, Soft Matter **5**, 4357 (2009).
[62]G. A. Voth, *Coarse-Graining of Condensed Phase and Biomolecular Systems* (CRC Press, 2008), ISBN: 978-1-4200-5956-4.
[63]W. G. Noid, J. Chem. Phys. **139**, 090901 (2013).
[64]M. S. Shell, J. Chem. Phys. **129**, 144108 (2008).
[65]A. Chaimovich and M. S. Shell, J. Chem. Phys. **134**, 094112 (2011).
[66]V. Rühle, C. Junghans, A. Lukyanov, K. Kremer, and D. Andrienko, J. Chem. Theory Comput. **5**, 3211 (2009).
[67]S. Y. Mashayak, M. N. Jochum, K. Koschke, N. R. Aluru, V. Rühle, and C. Junghans, PLoS ONE **10**, e0131754 (2015).
[68]D. J. Bonthuis, S. Gekle, and R. R. Netz, Phys. Rev. Lett. **107**, 166102 (2011).
[69]D. J. Bonthuis and R. R. Netz, J. Phys. Chem. B **117**, 11397 (2013).
[70]S. A. Adelman, J. Chem. Phys. **64**, 724 (1976).
[71]D. Levesque, J. J. Weis, and G. N. Patey, J. Chem. Phys. **72**, 1887 (1980).
[72]J.-P. Hansen and I. R. McDonald, *Theory of Simple Liquids* (Elsevier, 2013), pp. 455–510.
[73]A. Kohlmeyer, C. Hartnig, and E. Spohr, J. Mol. Liq. **78**, 233 (1998).